Journal of Renewable Materials
DOI:10.32604/jrm.2020.011327
Article

Tech Science Press

Component Optimization and Seepage Simulation Method of Resin Based Permeable Brick

Xiaofu Wang[1,*], Xiong Zhang[1], Yan He[2] and Chunming Lian[3]

[1]Key Laboratory of Advanced Civil Engineering Materials of Education Ministry, School of Material Science and Technology, Tongji University, Shanghai, 201804, China
[2]School of Civil Engineering, Suzhou University of Science and Technology, Suzhou, 215011, China
[3]China Construction Eighth Engineering Bureau Co., Ltd., Shanghai, 200122, China
*Corresponding Author: Xiaofu Wang. Email: 1710048@tongji.edu.cn
Received: 01 May 2020; Accepted: 01 June 2020

Abstract: In order to solve the problem of urban surface runoff, it is necessary to study permeable brick deeply. Tensile test and DMA test were used to study the binder material of permeable brick, and a material with the best mechanical properties was selected as the binder of resin based permeable brick; The permeable brick with single gradation and continuous gradation and porosity of 0.1–0.5 gradient is constructed by 3D modeling method. The particle composition and the seepage simulation results of permeable brick under different design parameters were analyzed; A resin-based permeable brick with micro-pores was prepared using the selected binder and desert sand with high roundness as aggregate, and compared with the simulation, its water permeability coefficient is 3.25×10^{-2} cm/s and the compressive strength is 36.19 MPa. In the seepage simulation of permeable brick, it is known that with the increase of gradation width "value *i*", the water permeability coefficient increases. Therefore, in order to control the number of aggregate particles and obtain better seepage performance, the wide gradation of $i \geq 4$ and the design porosity of 0.3–0.4 should be considered. This study provides a research basis and a simulation method for the component optimization of resin based permeable brick.

Keywords: Permeable brick; epoxy resin; aggregate; sponge city

Nomenclature

u_f:	Darcy velocity
k:	permeability coefficient
μ:	liquid viscosity
∇P:	pressure drop
V_f:	Forchheimer velocity
γ:	Forchheimer coefficient
ρ_f:	liquid density
σ_t:	tensile strength
P:	failure load

b: specimen width
h: specimen thickness
ρ_w: water density
E_t: tensile elastic modulus
ΔP: load increment of initial straight segment on load-deformation curve
ΔL: deformation increment in the gauge distance L_0 corresponding to the load increment ΔP
ε_t: elongation at break
ΔL_b: elongation within the gauge distance L_0 when the sample breaks
ε: porosity of permeable brick
ε': proportion of voids in 2D slices
m_{12}: wet weight of fully immersed permeable brick
m_{22}: dry weight of permeable brick
V: volume of permeable brick
i: aggregate particle grading width value

1 Introduction

The continuous transformation of human living environment makes urbanization an irreversible process, in the process of urbanization, the permeable surface of road surface is gradually replaced by the impermeable surface [1,2], this has brought many urban diseases such as waterlogging and heat island effect to the city [3–8]. To solve these problems, it is necessary to increase the proportion of permeable surface in the original urban surface, pervious pavement materials are needed in road materials. In the use of permeable pavement materials, the amount of permeable brick is very large, permeable brick is a kind of pavement material which constructs a large number of connecting channels in the brick body. The common permeable bricks at present are cement-based porous permeable brick and sintered porous permeable brick [9,10]. The research on cement-based permeable brick and sintered permeable brick has been carried out very early, but their shortcomings are obvious, such as: rough surface, poor wear resistance, long maintenance cycle; high preparation temperature, causing great pressure on the environment; large apparent pores are easy to block, short life cycle, etc., which also restrict the application of permeable brick as a kind of permeable pavement material. Therefore, it is urgent to develop a new permeable brick that can overcome the above defects.

Permeable brick is composed of framework and pore, framework provides a stable physical structure for permeable brick, and it is composed of aggregate and binder material. There are many researches on permeable brick aggregate, Mandula et al. [11] prepared permeable brick with permeability rate of 3.5×10^{-2} cm/s by using the particle with fine aggregate of 70% (particle size 0.6–2.36 mm) and coarse aggregate of 30% (particle size: 2.36–4.75 mm), Wang et al. [12] prepared cement permeable brick with permeable rate of 3.2×10^{-2} cm/s by using aggregate with particle size range of 3–5 mm. The grey correlation study of He et al. [13] on cementitious materials and aggregates showed that the gradation of aggregates has a great influence on the properties of permeable materials, and the effects of various factors on the effective porosity and permeability coefficient of concrete permeable brick are consistent: aggregate grading > aggregate cement ratio > water cement ratio > 0.6 (grey correlation degree). Through the design of aggregate gradation, the pore characteristics of porous media can be designed, such as porosity, pore size, etc., through the selection of aggregate shape, the pore shape can be further designed. The characteristics of pores will further affect the permeability and mechanical properties of permeable materials, Trablsi's et al. [14] research on pore size distribution of building materials shows that microstructure can affect the capillary phenomenon of materials. There are also many researches on the cementitious materials of porous materials. Zhu et al. [15] used the tailings mined by the mine as the

binder, and melted the tailings waste at 1180–1200°C for 45 min to prepare the permeable brick with a permeable rate of 3×10^{-2} cm/s, with 20 wt% tailings; Xie et al. [16] prepared permeable brick with permeable rate of 1.08×10^{-2} cm/s at 1150°C, using sludge from waterworks as binder and sand with particle size range of 1.0 mm–1.4 mm for 1 h; Shi et al. [17] used the mixture of sodium silicate solution, fly ash and quartz sand as cementitious material, and added the feldspar quartz tailing with the particle size of 7 mm–10 mm as aggregate to prepare the permeable brick with the permeable rate of 2.44×10^{-2} cm/s; He et al. [18] used P•O 42.5R ordinary portland cement and polycarboxylic acid water reducing agent and steel slag aggregate with a particle size of 4.75 mm–7.1 mm to prepare permeable brick with permeability coefficient of 4.2×10^{-2} cm/s, but the strength development of cement-based materials requires sufficient hydration of the cement. Only after curing to a certain age can the strength that meets the performance requirements [19–22]. Therefore, cement as a binder material for porous materials still has certain disadvantages.

In addition to the inorganic binder materials mentioned above, there are also organic binder materials. However, the use of organic binder materials in building materials mainly focuses on corrosion-resistant coating, prevention of chloride ion diffusion, defect repair and as an admixture [23–26], there are few studies on the use of porous brick and related research. In the study of organic adhesive materials, Prolongo et al. [27] used aluminum substrates to perform a shear test to study the bonding properties of different epoxy resins. The results showed that epoxy/aromatic amine system had higher adhesive strength (5.8 ± 0.3 MPa) and higher glass transition temperature ($Tg = 207$°C) than homopolymer resin system; Young et al. [28] added silica into the curing system of epoxy resin, and the results showed that the young's modulus of epoxy resin with brittle characteristics was significantly increased after adding silica; Rao et al. [29] studied the polyurethane resin (PU resin), which is formed by the crosslinking of isocyanate and polyol, the two components are the hard segment and the soft segment of the resin, and the resin with controllable mechanical properties can be prepared by controlling the ratio of the groups of the two components (-NCO/-OH), Trovati et al. [30] showed that when the mass ratio of isocyanate and polyol was 1:1, 1:1.5, 1:2.5, the resin was rigid, semi-rigid and soft. According to the research by Kostrzewa et al. [31] the epoxy resin can also be modified in the preparation process. The epoxy resin has performances of brittleness, poor crack propagation resistance and low elongation at break. In order to improve its flexibility, isocyanate (MDI) in polyurethane can be added into the epoxy resin. When 5%–10% polyurethane is added to epoxy resin, it can significantly improve the mechanical properties such as tensile resistance and shear resistance of epoxy resin, but the glass transition temperature will decrease. So, the organic adhesive material can be used as a binder material of porous material with its excellent adhesive ability and adjustable mechanical properties.

As we all know, there are three ways to solve practical problems in academic: (a) theory, (b) experiment, and (c) simulation. In the above three ways, theoretical research is the foundation of follow-up research and provides direction for them. Experimental research is the exploration of theoretical application and phenomenon, while simulation is the bridge between theoretical research and experimental research. Through simulation, the theory can better guide the experiment, and the experiment can better mine the defects of the theory. At the same time, many unpredictable realities can be obtained through simulation, such as very large macro experiments and micro properties of materials. Simulation can provide methods for optimization of experimental schemes and selection of theory. The simulation method can also be used in brick and porous materials. Araújo et al. [32] used ANSYS CFX software 15.0 to simulate the heat treatment of porous ceramic brick, and used Computational Fluid Dynamics (CFD) techniques, the results show that the thermal and quality fields of porous ceramic bricks are asymmetric in the process of heating treatment, and their properties highly depend on the placement of porous ceramic bricks, so it can be designed in the experiment or production. Thomas et al. [33] used Avizo software v.9.2 to simulate the clay mineral porous media, revealed the anisotropy of fluid migration in clay based materials, so this factor should be considered as much as possible during the compaction process. There are many different phenomena and corresponding theories of porous material seepage, such as turbulence caused by high

velocity and disturbance, which can be described by Navier-Stoke equation. Laminar flow is due to the direction of liquid flow parallel to the tube axis. Darcy's law can describe groundwater flow. With the change of liquid velocity, the Reynolds number is also changing. According to the different Reynolds number, the laminar and turbulent states of liquid can also be predicted. Due to the small Reynolds number in permeable brick, Darcy's law and Darcy-Forchheimer equation, which limit the Reynolds number to 240–280, can analyze the seepage state of brick [34]. The basic equation of Darcy's law is shown in Eq. (1), it can be seen from the formula that Darcy's law considers that there is a linear proportional relationship between pressure drop and flow velocity. Darcy-Forchheimer equation is shown in Eq. (2). When the Reynolds number increases, turbulence will occur. It makes a nonlinear correction on the basis of Darcy's law, but Darcy-Forchheimer equation still assumes that Darcy's law is valid before adding nonlinear correction [35]. Darcy's law was put forward by French engineer Darcy. In many subsequent researches involving porous media, this equation was adopted or modified according to the use situation. Brinkman equation can describe the rapid seepage of soil near the shaft wall in the underground water flow. In the state of multi physical field coupling, these equations can be transformed and used, such as flow heat coupling, etc. [36–39]. Therefore, the theoretical formula can be selected according to different conditions.

$$u_f = -\frac{k}{\mu}\nabla P \tag{1}$$

$$\nabla P = -\frac{\mu}{k}V_f - \gamma\rho_f\left|V_f\right|^2 V_f \tag{2}$$

Based on the above analysis, the following work is carried out in this paper:

Resin has excellent mechanical properties and convenient forming conditions. In this study, resin is used as the adhesive component of permeable brick, and desert sand with high roundness is used as the aggregate to prepare a resin based permeable brick (RBPB for short). This permeable brick is mainly permeable through the pores between the sand particles. Two different resins were studied by tensile test and DMA, and a resin binder material with better mechanical properties and simple preparation conditions was selected. The three-dimensional modeling method is used to design the parameters such as porosity and aggregate gradation, and different porous media are constructed. On this basis, the Brinkman equation theory model is used to simulate the seepage characteristics of porous media, and compared with the actual situation, a method of aggregate selection is obtained, which provides research support for the optimization of permeable brick aggregate.

The research route of this paper is shown in Fig. 1.

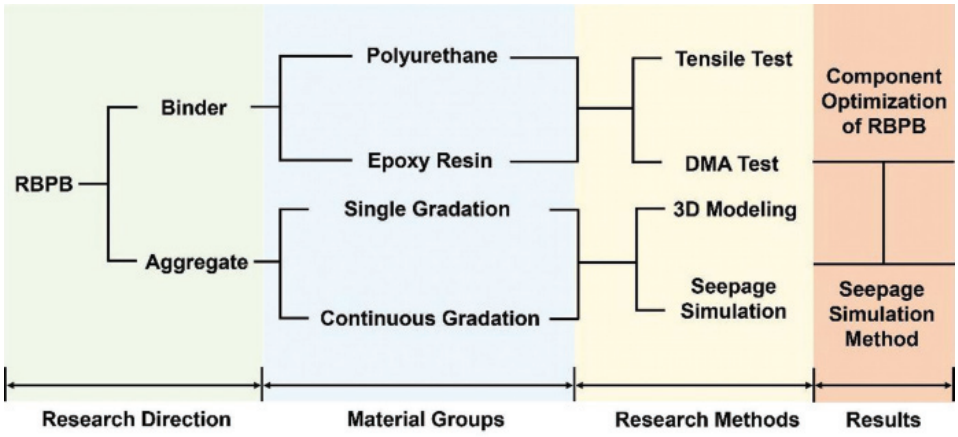

Figure 1: Research route

2 Experimental

2.1 Raw Material

The raw materials of RBPB include resin binder and aggregate. E51 epoxy resin and polyurethane (PU for short) are selected in the use of binder materials. Component A of epoxy resin is bisphenol A epoxy resin with epoxy value of 0.51, component B is amine curing agent (adduct of diethylenetriamine and butyl glycidyl ether), total amine value is 500~700 mg KOH/g, The mixing ratio of component A and component B is 100:30. PU binder was developed by BASF Polyurethane Specialties (China) Company Ltd., (BASF). A pre-calculated amount of part-A was mixed with part-B at a ratio of 100:60 using a vacuum mixer at 2050 rpm for 2 min at room temperature, where part-A refers to polyol and part-B refers to isocyanate. In order to obtain the permeable brick with better appearance, the sand with higher roundness is selected as the aggregate. According to the screening test, the particle size of aeolian sand aggregate is mainly 0.5 mm, and its mass ratio is 78.486%.

2.2 Mechanical Test for Resin

2.2.1 Tensile Test for Resin

SANS CMT7000 universal testing machine was used for tensile test of resin casting, which is from MTS systems (China) Co., Ltd. The preparation method of samples shall be in accordance with the national standard GB/T 2567-2008 [40] Test method for properties of resin casting body, prepare the test materials according to the predetermined curing system under the condition of room temperature 15°C~30°C and relative humidity less than 75%. After pouring, the mold is placed at room temperature for 24~48 h and then demoulded. After demoulding, open the sample on the plane, and place it at room temperature or standard ambient temperature for 504 h (including sample processing time), and the tensile test shall be carried out after standard size grinding of the specimens.

When measuring the tensile strength, the test speed is 10 mm/min and the arbitration test speed is 2 mm/min; when measuring the elastic modulus and stress-strain curve, the test speed is 2 mm/min.

The tensile strength is calculated according to Eq. (3):

$$\sigma_t = \frac{P}{b \cdot h} \tag{3}$$

The tensile elastic modulus is calculated as Eq. (4):

$$E_t = \frac{L_0 \cdot \Delta P}{b \cdot h \cdot \Delta L} \tag{4}$$

The elongation at break is calculated according to Eq. (5):

$$\varepsilon_t = \frac{\Delta L_b}{L_0} \times 100 \tag{5}$$

2.2.2 Dynamic Mechanical Analysis (DMA)

DMA tests were conducted on a TA Q800 dynamic mechanical analyser at the frequency of 1 Hz, temperature range of 20–150°C, and the heating rate was set at 2 k min^{-1}, and the modulus test is three-point bending. The size of the specimens was 5 mm × 10 mm × 50 mm. The viscosity-temperature behavior was observed and the glass transition temperature (Tg) points were calculated.

2.3 Simulation Method of RBPB

2.3.1 3D Modeling

Setting the boundary can make the particles generated in the closed three-dimensional space according to the specified requirements. The porosity and particle size of the permeable brick are designed. The PFC 3D software is used for three-dimensional modeling. The process of model generation and post-processing is shown in Fig. 2.

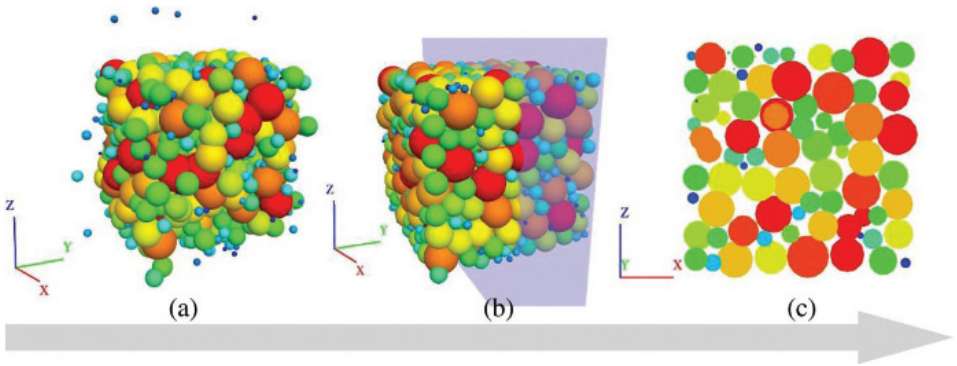

Figure 2: 3D modeling and z-x plane slicing. (a) Model generation process, (b) Slicing process of the z-x plane of the three-dimensional model, (c) Schematic representation of the slicing plane

Single gradation research: permeable bricks were modeled according to porosity of 0.1, 0.2, 0.3, 0.4, 0.5. The particle size of single graded permeable brick is 0.5 mm, which is the highest proportion of desert sand particles.

Continuous gradation research: take $i = 1$ for every 0.1 mm of grain size, select the grading distribution shown in Tab. 1 for modeling, since the particle distribution of the continuous gradation can be regarded as a Gaussian distribution, the distribution of the generated particles follows the Gaussian distribution and set the porosity gradient to 0.1, 0.2, 0.3, 0.4, 0.5 for modeling.

The optimal particle size and pore gradient were selected from the above models for further modeling.

Table 1: Distribution rules of continuous graded particles

Distribution width	Grain Size/mm
i = 10	0.1–1
i = 8	0.2–0.9
i = 6	0.3–0.8
i = 4	0.4–0.7
i = 2	0.5–0.6

2.3.2 Seepage Simulation

In the software, the z-x plane of the three-dimensional model permeable brick is sliced, and ten groups of permeable brick's slices are binarized, then the simulation software COMSOL 5.3 is used to simulate the

hydrodynamics. The physical field interface is "Fluid Flow", and the Brinkman-Forchheimer equation is used to model.

2.4 Test Method for Water Permeability and Mechanical Properties of RBPB

Test methods and indicators for the permeability of water-permeable materials refer to GB/T 25993-2010 [41], The sample is drilled into a cylinder of φ75 × 50 and its permeability is tested with a water head tester conforming to Darcy's law specified by national standards. The mechanical property test shall refer to GB/T17671-1999 [42], and a universal testing machine was used to obtain the compressive strength with the loading rate of (2400 ± 200) N/s.

3 Results and Discussion

3.1 Test Results of Binder Materials

3.1.1 Tensile Test

The width, thickness and original gauge distance of the tensile specimen are 10 mm × 5 mm × 80 mm, the test is performed according to the standard GB/T 1040-92 [43]. Yao's et al. [44,45] research on the mix design of cementitious materials for construction engineering is very in-depth, and a strength prediction model based on mix proportion is proposed. Therefore, the mix proportion has a great influence on the strength, and the proper mix proportion is crucial to the performance of the material. In this paper, the mix proportion selected according to the curing properties of the resin is shown in Tab. 2.

Table 2: Mix proportion of test pieces for tensile test of binder materials

Grade	Resin/g	Curing agent/g	Total mass/g
E51	80	20	100
PU	61	39	100

Table 3: Tensile test data

Grade	Maximum force/N	Elongation at break/%	Tensile fracture stress/MPa	Tensile strength/MPa
E51	2414.41	5.25	54.87	54.87
PU	596.45	13.52	6.05	11.47

Tab. 3 is the basic data of tensile test for resin casting.

As shown in Tab. 3, the tensile strength of E51 reached 54.87 MPa, while the tensile strength of castings made of polyurethane was only 11.47 MPa. Epoxy resin is superior to polyurethane in terms of crosslinking density and strength of polymer. The elongation at break of bisphenol-A epoxy resin is more than half smaller than PU, so epoxy resin is more brittle, while polyurethane has better ductility. Therefore, the brittleness, toughness and tensile strength of the binder materials should be fully considered in the selection of the binder materials for permeable pavement. The stress-strain curves of the two binder materials are shown in Fig. 3.

Fig. 3 is the stress-strain curve of the two resins. From Fig. 3a, it can be seen that the stress-strain curve of E51 has only a rising section and no falling section; In Fig. 3b, it can be seen that the stress-strain curve of viscoelastic material has the characteristic of elastic deformation stage, yield stage, strengthening stage and local shape changing stage. $\sigma = 9$ MPa, which is the yield point of PU resin. It can be seen from Fig. 3 that bisphenol A epoxy resin is closer to brittle material and only accepts partial elastic deformation. PU material is an elastic-plastic material, when the material exceeds the yield point, although the processing

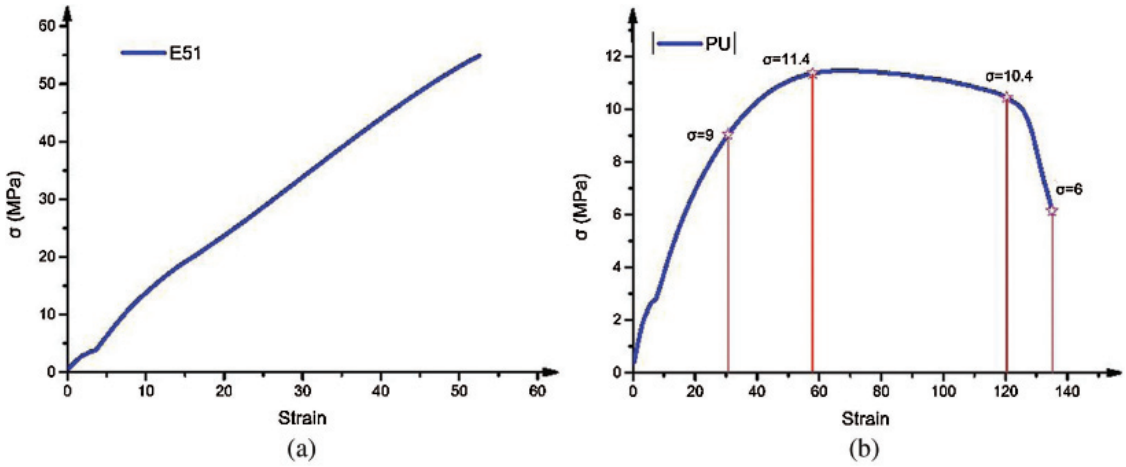

Figure 3: Stress-strain curve of resins (a) Stress-strain curve of E51 resin, (b) Stress-strain curve of PU

strengthening will lead to the generation of the maximum stress, but the irreversible plastic deformation will lead to the damage of the material structure, and its maximum strength value is lower. When testing the binder material of the "sponge city" permeable material, the data of yield stress should be used instead of the maximum stress and failure stress. By comparison, it can be seen that PU has strong deformation ability but low yield stress value. It is not suitable to use PU material as binder material when preparing "sponge city" water-permeable materials.

In the analysis of the mechanical properties and toughness of materials, in addition to analyzing the stress-strain curve, the modulus and compliance should be quantitatively analyzed. The elastic properties and brittleness of the material can be judged by measuring the change of modulus and compliance under the external load, and the deformation rate of each unit index of the material can be observed through the index of Young's modulus.

Young's modulus is a physical quantity describing the resistance of a solid material to deformation. It is defined as the ratio between uniaxial stress and uniaxial deformation within the range applicable to Hooke's law. Therefore, E51 resin can be plotted at all measurement points, while PU resin can only be plotted before the yield point. If it exceeds the yield point, plastic deformation occurs, which does not comply with Hooke's law. From Fig. 4a, it can be seen that after the rapid decline of the two resin binder materials in the initial

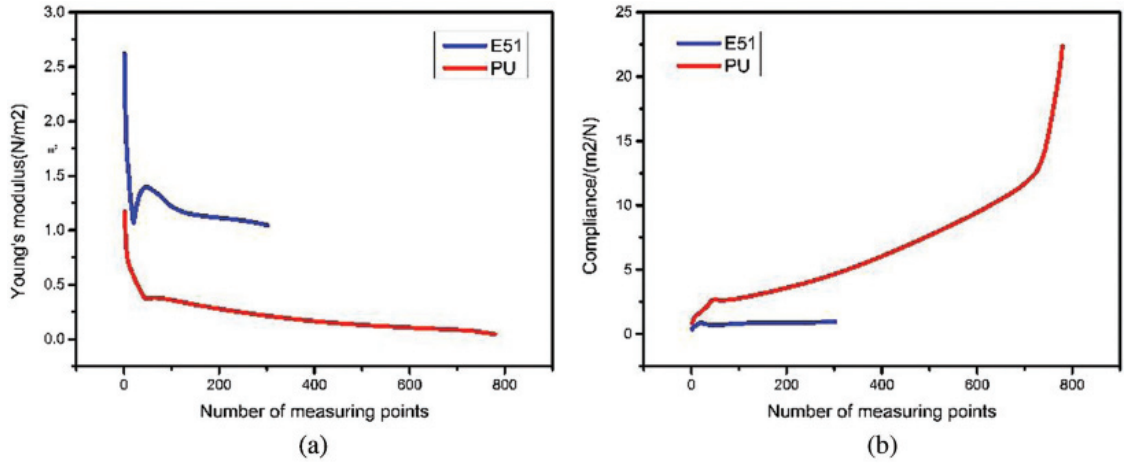

Figure 4: Modulus and compliance of resins (a) Young's modulus of resins (b) Compliance of resins

stage, E51 tends to be flat after one rise, PU does not rise obviously, but it also tends to be flat. At the end of the measuring point, it can be seen that the Young's modulus of the two cementitious materials is in the order of E51 > PU, Therefore, the stiffness and brittleness of bisphenol A epoxy resin is higher, while the flexibility of PU is higher. It is worth noting that the rapid decrease of Young's modulus at the beginning is the transition stage of stress on the spline at the beginning of tensile test, which should be ignored, while the measurement point is a description of time step.

Tensile compliance is an elastic constant, which is equal to the ratio of strain to stress. It is the deformation rate per unit stress of the material. Therefore, the intrinsic characteristics of the material can also be reflected from the compliance diagram, as shown in Fig. 4b In the compliance order, PU > E51, the result is opposite to the elastic modulus, so the conclusion is the same as above.

3.1.2 DMA

In the above study, the tensile fracture test have been performed on bisphenol-A epoxy resin and PU. Next, the storage modulus, loss modulus, glass transition temperature and tangent value of lag angle of bisphenol-A epoxy resin and PU resin can be obtained through dynamic thermomechanical analysis, as shown in Fig. 5.

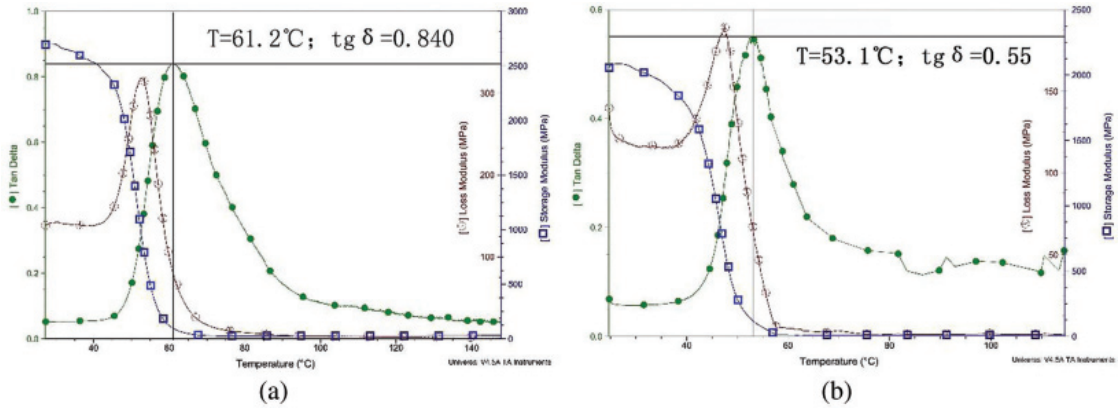

Figure 5: DMA results of two different binder materials. (a) Dynamic Mechanical Analysis of E51, (b) Dynamic Mechanical Analysis of PU

It can be seen from Fig. 5 that the storage modulus and the loss modulus of the two cementitious materials. The loss modulus exceeds the storage modulus between 40°C and 60°C, but the modulus loss value of PU resin is significantly higher than that of E51 resin, so the thermodynamic stability of PU resin is worse than that of E51 resin. The glass transition temperature of bisphenol A epoxy resin is 61.2° C, and the tgδ is 0.840, but the two values of PU resin are relatively low. Therefore, the high temperature resistance of E51 resin is better than that of PU resin. According to Tan Delta value, it can be known that the molecular chain of E51 resin is more rigid than that of PU resin. Therefore, the applicable temperature of such binder materials is within 61°C.

3.2 Modeling Results

In the 3D models, a linear-based model provide a standard bonding behavior in the parallel bonds between particles. These bonds can be installed at both ball-ball and ball-facet contacts. Both bonds can be envisioned as a kind of glue joining the contacting pieces just like the binder in the permeable bricks. The bond glue is of a finite size that acts over a cross-section lying between the contacting pieces. The bonds can transmit both a force and a moment.

3.2.1 3D Model of Single Gradation

The three-dimensional models modeled according to the porosity designed is shown in Fig. 6.

It can be seen from Fig. 6 that when the porosity is set to 0.1, in order to meet the porosity parameters, there is a large compression deformation between the particles, and in the sectional view of the ZX plane, it can be seen that the particles are squeezed by each other and the pores in the model had become closed pores. Therefore, when the porosity is set to 0.1, the situation reflected in reality is that the brick compression ratio is too large and the particles are crushed. For the seepage, the increase of ineffective pores results in predictable imperviousness and loss of the functionality of the permeable brick.

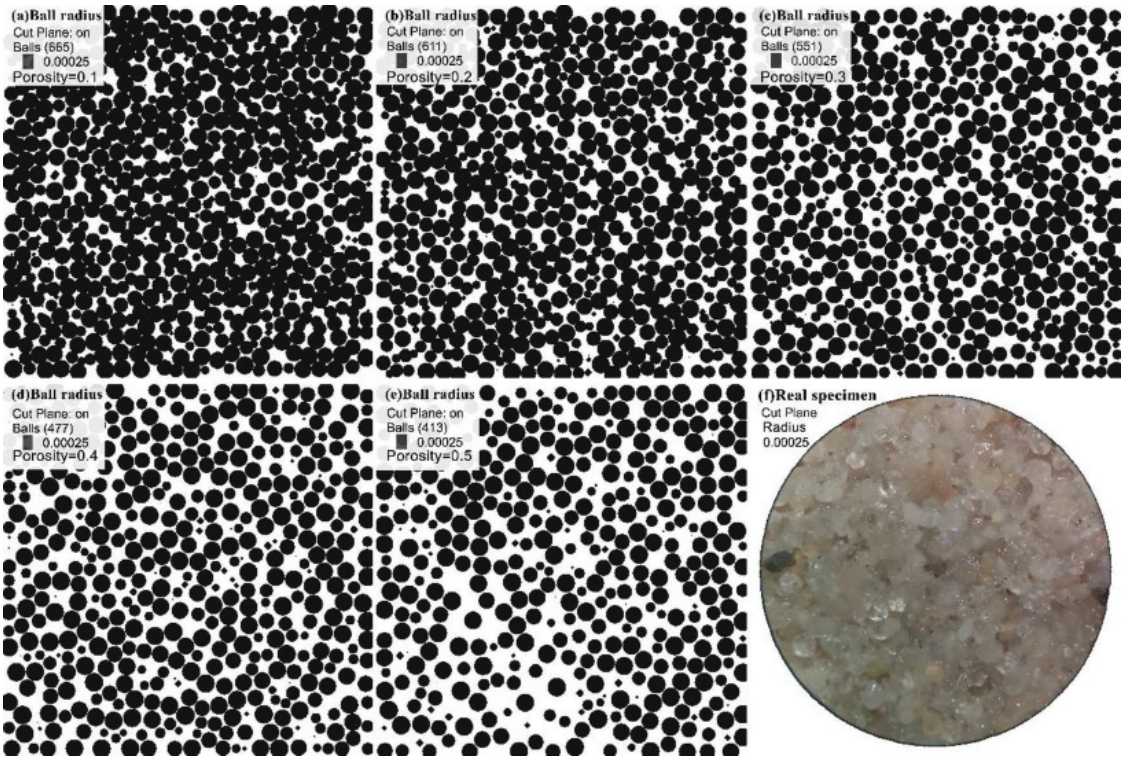

Figure 6: Grain Size = 0.5 mm, (a) $\varepsilon = 0.1$, (b) $\varepsilon = 0.2$, (c) $\varepsilon = 0.3$, (d) $\varepsilon = 0.4$, (e) $\varepsilon = 0.5$, (f) The real specimen made of desert sand which has grain size of 0.5 mm

When the porosity is 0.5, only the loose accumulation of particles cannot meet this set parameter. Therefore, the set porosity value can only be satisfied when a part of the space is left inside the brick body. In reality, the compression ratio is too low, and even bricks cannot be compacted due to lack of material. It can be predicted that the water permeability is good, but the strength can not meet the requirements. The proportion of white area, the area where the cavity is located, can be calculated from the pixels of 5 groups of pictures shown in Fig. 6, as shown in the following table. At the same time, with the increase of porosity, the whole particle number shows a linear downward trend, as shown in Fig. 7.

It can be seen from Tab. 4 that the design porosity of the three-dimensional model is not completely consistent with the void ratio of the two-dimensional slice, but it is relatively close. This is because when the design porosity is lower than 0.3, in order to reach the design value, the particles are squeezed into each other and the particles are squeezed into the wall. When the design porosity is greater than or equal to 0.3, the two kinds of porosity are gradually approach. This deviation is consistent with the actual situation.

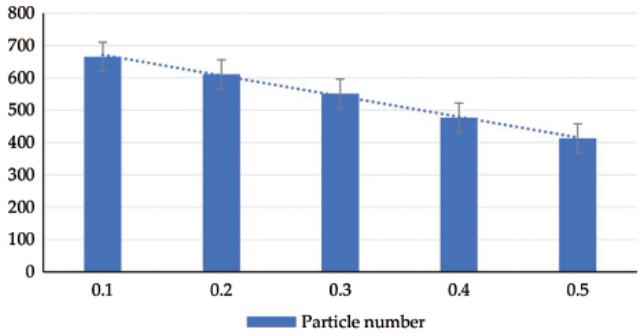

Figure 7: Change of particle number in three-dimensional model slice (Grain Size = 0.5 mm)

3.2.2 3D Model of Continuous Gradation

Based on the research in the three-dimensional modeling, it is difficult to meet the actual demand when the porosity $\varepsilon = 0.1$ and the porosity $\varepsilon = 0.5$. Therefore, the porosity of 0.3 was selected in the continuous grading modeling. The 3D models and the slices of them in z-x plane is shown in Fig. 8.

It can be seen from Fig. 9 that with the decrease of *i* value, the width of continuous grading of particles decreases gradually, but the number of particles increases continuously, which is a very interesting phenomenon. It should be noted that the porosity is the same in this group of tests, which is $\varepsilon = 0.3$, so the total volume of particles in each group of models should account for 70% of the brick, From the volume formula of the sphere $V_{ball} = \frac{4}{3}\pi r^3$ it can be known that the influence of the radius of the sphere on the volume has a cubic relationship, so the largest effect on the number of particles should be the part with the largest radius in the particles. As the i value decreases during the modeling process, the maximum particle size also decreases, so there is more volume allocated to small particles, so the number of particles almost rises in a straight line, at the same time, it affects the morphology of slices.

Therefore, a conclusion can be drawn here: when the design porosity is consistent, the influence of continuous graded aggregate conforming to Gaussian distribution on permeable brick is mainly concentrated on the value of maximum particle size, and the larger the maximum particle size is, the less the total number of particles is. The influence of aggregate particles on seepage is shown in the following study.

3.3 Seepage Simulation Results

In the process of three-dimensional modeling, it can be seen that the rationality of porosity design has a strong impact on the structure of the brick, so in the simulation of seepage situation, the model with connected pores should be reasonably selected for simulation. Take the z-x plane of three-dimensional image, and then perform seepage simulation. Firstly, the slice image is binarized, then inverted, and the pixel distribution of the imported image is identified by interpolation function to obtain porosity and pore distribution, where px represents the pixel distribution function of the image, and the x and y values in the formula can locate the position in the image, when positioning to the pore position, px(x, y) = 0 then $\varepsilon = 1$. 0.99 is the coefficient of smoothing the connection between pores and particles. The formula is shown in Eq. (6). The fluid pressure at the inlet is a 10 cm high head pressure in accordance with the national standard GB/T 25993-2010, and the pressure calculated according to Eq. (7) is 1000 Pa.

$$\varepsilon = 1 - 0.99 \times \mathrm{px}(\mathrm{x}, \mathrm{y}) \tag{6}$$

$$\mathrm{P} = \rho_w \mathrm{gh} \tag{7}$$

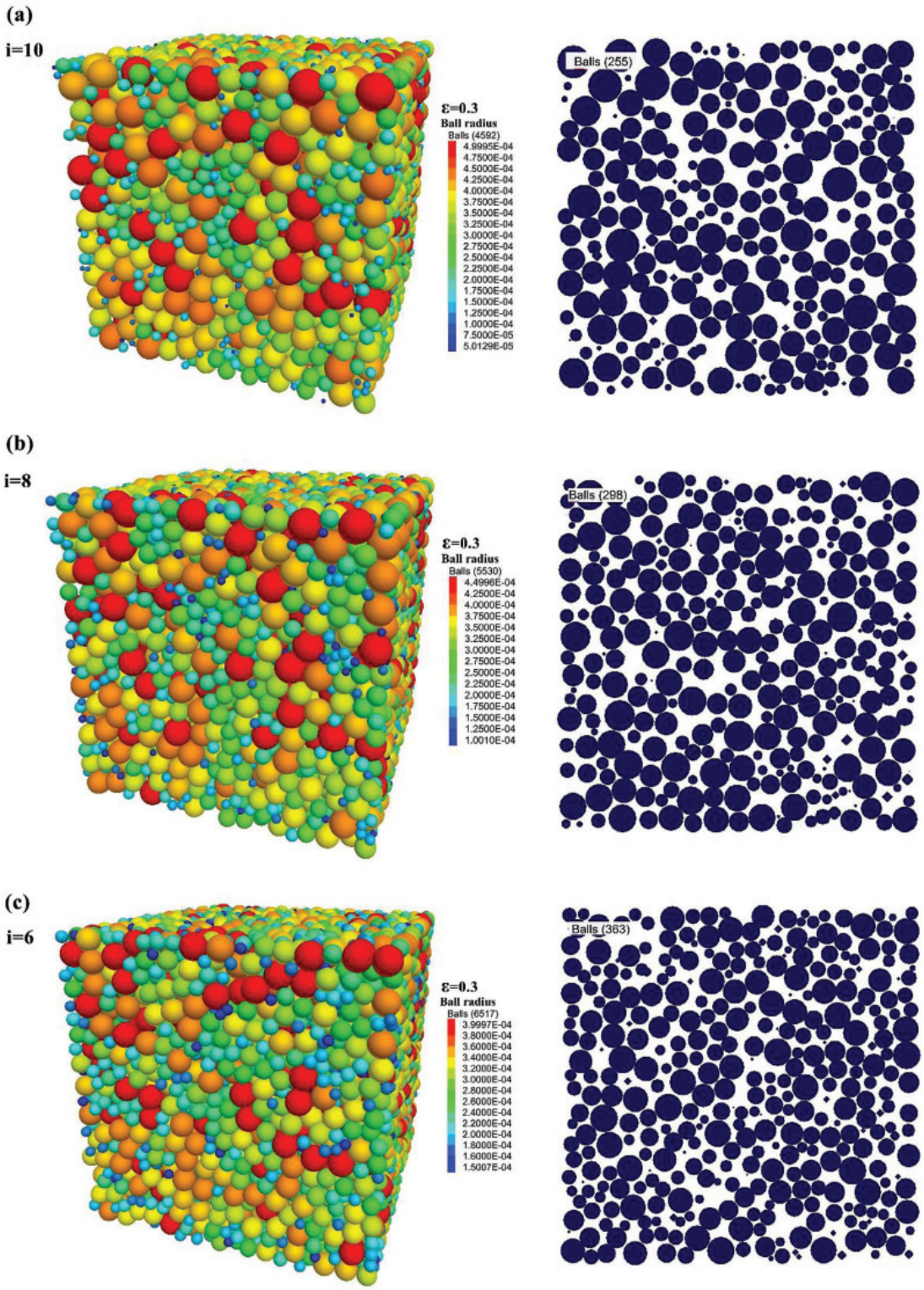

Figure 8: Part 1. Three dimensional models and slices with different *i* values when $\varepsilon = 0.3$, (i = 10, i = 8, i = 6)

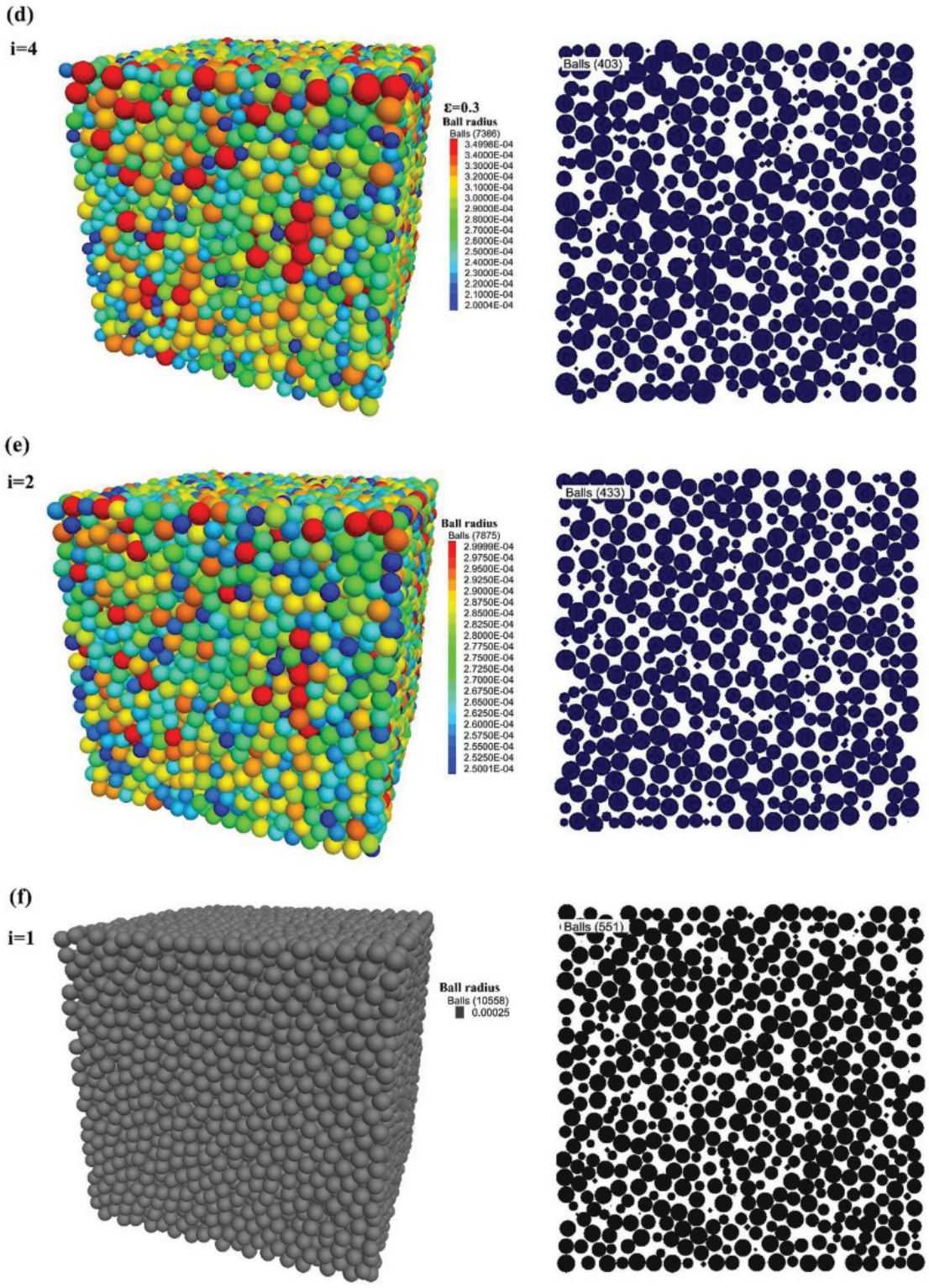

Figure 8: Part 2. Three dimensional models and slices with different *i* values when $\varepsilon = 0.3$ (i = 4, i = 2, i = 1)

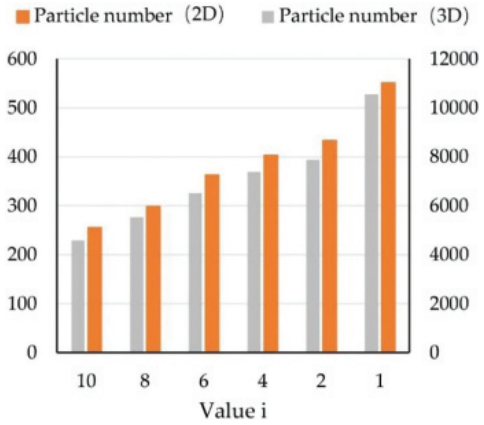

Figure 9: Change of particle number of brick in 2D and 3D models

Table 4: Proportion of voids in 2D slices

ε	White zone (pixel)	Whole picture (pixel)	ε'
0.1	3658112	22953320	0.159372
0.2	5426931	22953320	0.236433
0.3	7315788	22953320	0.318725
0.4	9618385	22953320	0.419041
0.5	11391115	22953320	0.496273

Table 5: Seepage results of single graded aggregate

i	Grain size/mm	Designed porosity/%	Maximum flow rate/$\times 10^{-2}$ cm/s	Minimum flow rate/$\times 10^{-2}$ cm/s	Particle number
1	0.5	0.1	0.52546	1.92E-07	13268
1	0.5	0.2	3.4625	9.95E-07	11982
1	0.5	0.3	4.33125	4.33E-07	10558
1	0.5	0.4	4.86497	6.24E-06	9097
1	0.5	0.5	4.66283	1.18E-05	7613

3.3.1 Seepage Results of Single Graded Aggregate

The particles with the grain size of 0.5 mm are used for simulation calculation according to the design porosity of 0.1, 0.2, 0.3, 0.4, 0.5, and the calculation results are shown in Tab. 5.

It can be seen that the flow velocity in the brick constructed with single particle size is greatly affected by the change of porosity and particle number. When the particle size is the same, with the increase of porosity, the number of particles in the brick will inevitably decrease, the effective porosity will increase, resulting in the increase of flow velocity. The simulation and flow rate are shown in Fig. 10.

Permeable bricks with a design porosity of 0.4 have a water permeability reaching 4.86497×10^{-2}cm/s, From Figs. 10a and 10b, it is obvious that the maximum flow rate will increase as the design porosity increases and the total number of particles decreases. It can be seen from Fig. 10c that

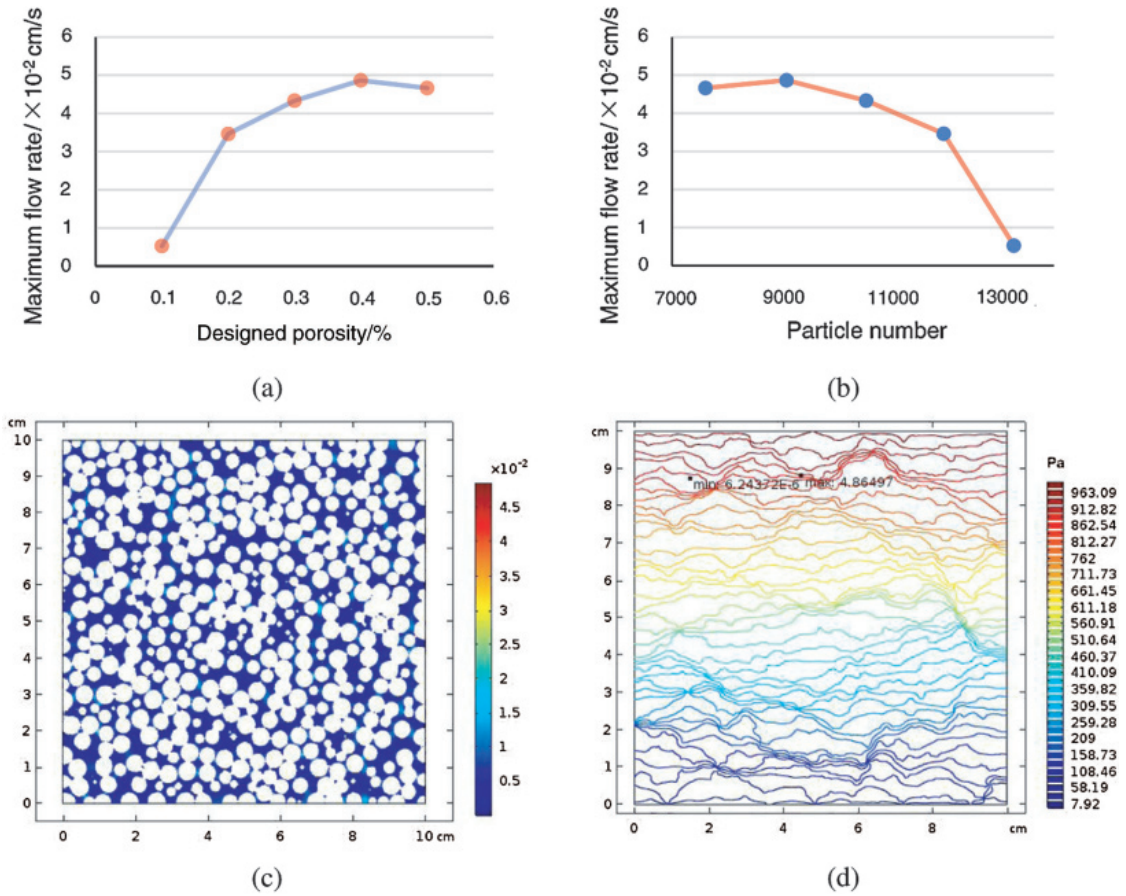

Figure 10: Simulation results of seepage of single size aggregate. (a) Relationship between porosity and maximum velocity, (b) Relationship between the number of particles and the maximum flow rate, (c) 0.5–0.4 Velocity of flow, (d) 0.5–0.4 Pressure drop

the bricks have uniform pores and uniform flow velocity. It can be seen from Fig. 10d that the pressure drop of the brick is also very uniform, the isobar is uniform, and the maximum flow velocity appears near the surface layer.

3.3.2 Seepage Results of Continuous Graded Aggregate

According to the above research, the porosity of 0.3 is used in the continuous grading test, the *i* values were 10, 8, 6, 4, and 2 for simulation. The results are shown in Tab. 6.

According to the conventional thinking, when the design porosity is the same, the flow velocity should be close, but it is not so from the seepage simulation results of the continuous graded aggregate. With the decrease of *i* value, the maximum flow rate and the minimum flow rate also decrease, while the total number of particles increases. It is proved that the width of continuous gradation has a definite effect on the velocity. Flow rate and simulation results are shown in Fig. 11.

From Figs. 11a and 11b, it is found that *i* value has a negative correlation with the total number of particles in the brick, during the process of *i* value decreasing, the total number of particles is increasing, and the maximum flow rate is gradually decreasing. Figs. 11c and 11d is a set of simulation diagrams when $i = 4$. It can be seen that after the aggregate gradation is appropriately widened, the maximum flow rate has exceeded the single-graded permeable brick, and the velocity of permeable brick with larger *i*

Table 6: Seepage simulation results of continuous graded aggregate

i	Grain size/mm	Designed porosity/%	Maximum flow rate/$\times 10^{-2}$ cm/s	Minimum flow rate/$\times 10^{-2}$ cm/s	Particle number
10	0.1–1	0.3	7.8438	4.23E-06	4592
8	0.2–0.9	0.3	7.8414	1.97E-06	5530
6	0.3–0.8	0.3	5.6429	1.46E-06	6517
4	0.4–0.7	0.3	4.9844	2.22E-06	7386
2	0.5–0.6	0.3	4.8404	1.42E-08	7875

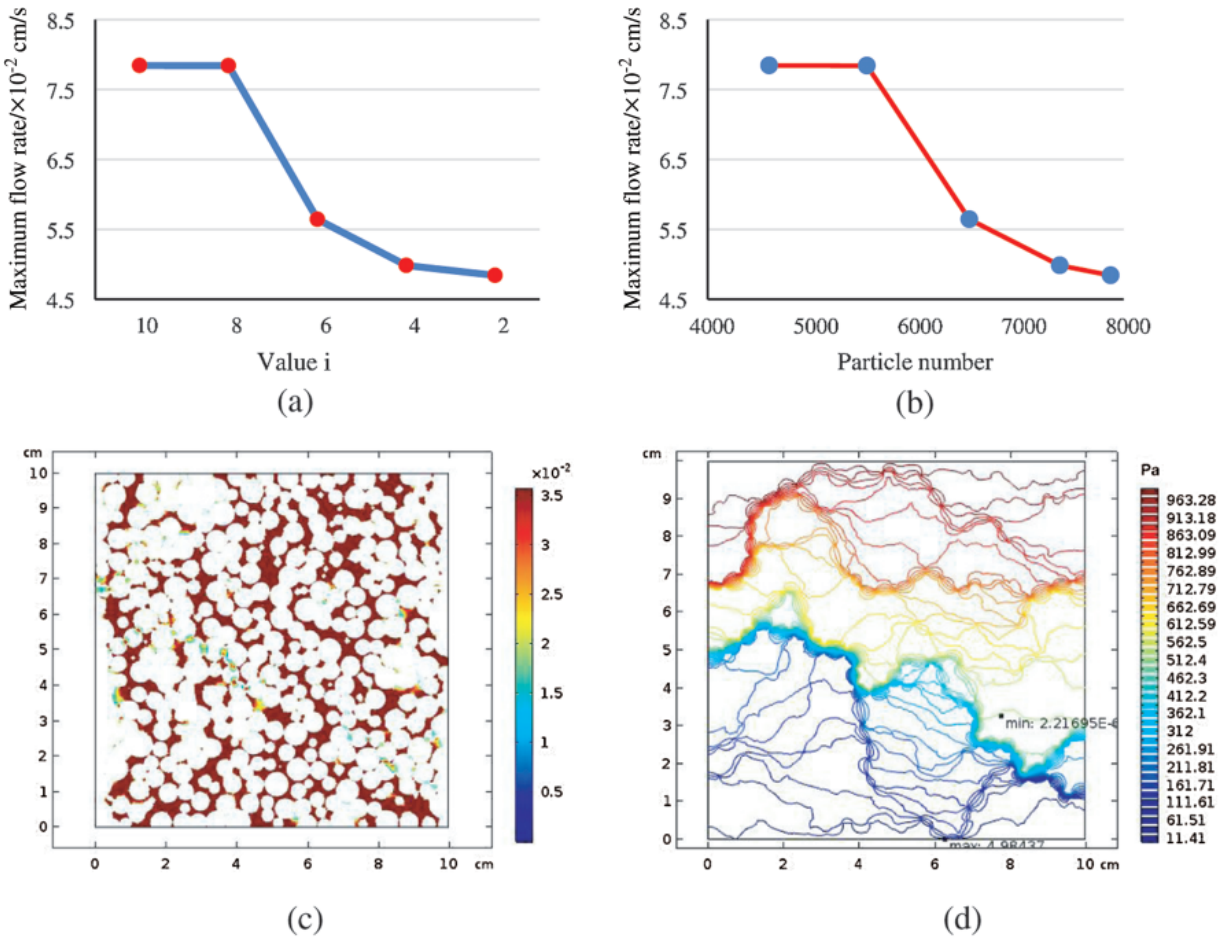

Figure 11: Simulation results of seepage of continuous graded aggregate. (a) Relationship between *i* value and maximum flow rate, (b) Relationship between the number of particles and the maximum flow rate, (c) 0.4–0.7–0.3 Velocity of flow, (d) 0.4–0.7–0.3 Pressure drop

value has far exceeded that of permeable brick with single particle size. The pressure drop is more obvious than that of single-graded aggregate bricks, and the place with the highest flow velocity appear in the final drainage of the brick.

3.4 Basic Properties and Micro Analysis of RBPB

3.4.1 Water Permeability and Mechanical Properties of RBPB

The permeable brick made of desert sand and epoxy resin, in the preparation of bricks, sand is used as aggregate, and epoxy resin system is used as binder material. Their mix proportion is shown in Tab. 7.

Table 7: The mix proportion of resin based permeable brick

Composition	Sand	Resin	Curing agent
Weight fraction (wt%)	94.30	4.56	1.14

When the total volume of porous materials is constant, the mechanical properties increase with the increase of the content of binder materials, but the water permeability will decrease. Through some exploration experiments, it was found that the mechanical properties cannot meet the requirements when the mass ratio of the binder is lower than 2%, and the water permeability cannot meet the requirements when the mass ratio is higher than 8%. Therefore, considering the mechanical properties, water permeability and cost, the proportion of the total mass of resin and curing agent accounting for 6% of the aggregate is used for subsequent research, and the proportion of curing agent and resin is as follows:

$$m(curing\ agent):m(\text{resin}) = 1:4 \tag{8}$$

RBPB has a permeability coefficient of 3.25×10^{-2}cm/s and a compressive strength of 36.19 MPa. Refer to Jiang's method [46], According to Eq. (9), the porosity of permeable brick is 30.39%. It can be seen that the permeability coefficient of permeable brick completely exceeds the national standard, which is equivalent to the maximum velocity of single particle permeable brick with a design porosity of 0.2 in seepage simulation. It should be pointed out that there should be a certain difference between the permeability rate of permeable brick in the actual situation and the maximum velocity in the ideal situation. The measured value reflects the average velocity in the steady state. Although it is a steady-state simulation, the phenomenon of maximum flow rate occurs. This is because the change in the diameter of the fluid channel and the unevenness of the pore distribution will lead to the tortuosity and fluid obstruction of the fluid channel. According to the measured porosity, the difference between the measured value and the simulated maximum velocity is 1.08×10^{-2} cm/s.

$$\varepsilon = \frac{m_{12} - m_{22}}{V \cdot \rho_w} \times 100\% \tag{9}$$

3.4.2 SEM Analysis for RBPB

SEM was used to study permeable brick, and the results are shown in Fig. 12.

It can be seen from Fig. 12 that the roundness of aeolian sand particles is high, so it is reasonable to consider it as a sphere in the modeling. It can be seen in the SEM image that the particle overlap pores and large gaps are consistent with the slice map in the modeling. There are brittle fracture defects caused by grinding cyclic stress at the joint of aggregate and resin. The calculation formula of roundness is: the area of particle projection divided by the area of circle with projection perimeter as its perimeter. The simplification formula is as follows:

$$\text{Roundness} = \frac{4 \times \pi \times \text{Area}}{\text{Perimeter}^2} \tag{10}$$

Image Pro Plus software was used to calculate more than 100,000 particles, the average roundness of this desert aeolian sand is 0.92. As shown in Fig. 12, the roundness of one of the particles is about 0.93. Image

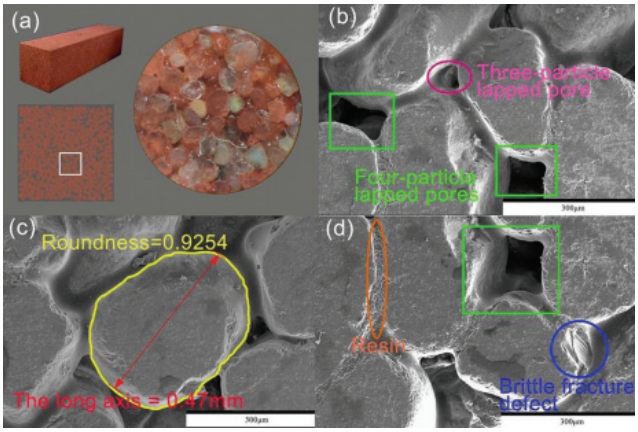

Figure 12: Micrograph of permeable brick specimen. (a) Physical picture, slice and model slice of RBPB, (b) Two different types of pores, (c) Roundness and long axis of particle, (d) Resin and brittle fracture defects

Table 8: SEM image data processed by Image Pro Plus software

Item	Area	Diameter (Max)	Diameter (Min)	Diameter (Mean)	Perimeter	Roundness
Pixels	440370	848.6301	618.7681	743.7935	2445.4170	0.9254
Length (mm)	0.1339	0.4680	0.3412	0.4102	1.3486	0.9254

analysis data is shown in Tab. 8. From Tab. 8, it can be seen that the long axis length of particles is 0.47 mm, the short axis length is 0.34 mm, and the average value is 0.41 mm, in which the long axis length is close to 0.5 mm, which is the diameter of simulated particles. In addition, the pore size of the lapped pores is 30–100 microns, of which the three-particle lapped pore diameter is 30–50 microns, and the four-particle lapped pore diameter is 100 microns. Kayhanian's et al. [47] study shows that when the diameter of harmful particles is larger than 38 microns, permeable concrete will be blocked, while Siriwardene's et al. [48] study shows that when the diameter of particles is smaller than 6 microns, particles in porous media will migrate with water, and a deposit layer will be formed at the bottom of porous materials to prevent water from penetrating underground. The permeable bricks prepared in this study have two micron-level pores, which have smaller pore sizes than millimeter-scale permeable bricks, their existence will make RBPB have a complex three-dimensional network-like pore structure, which can effectively block the clogging and migration of harmful particles, making the permeable pavement service life longer. Besides,the small pore size of the surface layer is good for blocking large particles, it is also easy to be covered by small particle dust, but it can be solved by washing with some small high-pressure water guns.

3.5 Industrial Production and Application of RBPB

The permeable brick was successfully developed using epoxy resin and desert sand. The prepared permeable brick has been successfully used in pavement engineering in Xiamen, China. The production and application of resin-based permeable brick are shown in Fig. 13.

The mechanical properties and water permeability of permeable bricks prepared by using desert aeolian sand and epoxy resin in this study are greater than the national standards, and after 25 freeze-thaw cycles, the mass loss and strength loss are less than 13.5%. The advantages over other types of permeable bricks are shown in Tab. 9:

Figure 13: Production and application of resin-based permeable bricks

Table 9: Performance comparison of permeable bricks

Item	Permeability rate ($\times 10^{-2}$ cm/s)	Permeability aging (frequency)	Compressive strength (MPa)	Comprehensive evaluation
Resin-based permeable brick	≥3.0	>10 times	≥35	High durability and water permeability
Sintered permeable brick	≥1.0	<5 times	<35	High price and energy consumption
Cement-based permeable brick	≥1.0	<5 times	<30	High maintenance costs

Note: Permeability aging (frequency) refers to the experiment of RBPB on the filtration of fine particles, according to industry standard JG/T 376 [49].

Through the investigation, the performance parameters of three kinds of permeable bricks commonly found in the Chinese market are shown in Tab. 9. Resin-based permeable brick has various properties that surpass sintered permeable brick and cement-based permeable brick. At the same time, the preparation time and maintenance time of RBPB are short, which is enough to solve the problems of goods storage and logistics, and save the turnover space for the factory.

4 Conclusions

After the test of binder material and the simulation of aggregate, the following conclusions can be drawn:

1. It is feasible to choose epoxy resin as the adhesive material of permeable brick. The maximum breaking strength of epoxy resin is 54.87 MPa, its glass transition temperature is 61.2°C, and it has excellent mechanical properties and certain heat resistance.
2. When the design porosity is the same, the influence of continuous graded aggregate obeying Gauss distribution on permeable brick is mainly in the size of the maximum particle size. When the maximum particle size is larger, the total number of particles is fewer.
3. The wider the gradation distribution is, the larger the maximum particle size is, the faster the maximum velocity of permeable brick is. the maximum velocity of permeable brick made of single graded particles

is slower than that made of wide graded particles. In order to control the number of particles and obtain better seepage performance, the wide gradation of $i \geq 4$ should be considered, and the design porosity should be 0.3–0.4.

4. The average roundness of the desert sand particles is 0.92, and the long axis length is about 0.5 mm; the pores of the brick are mainly composed of three-particle overlapping pores and four-particle overlapping pores, and the pore size range is 30–100 microns, which can effectively prevent harmful particles from clogging or internal migration inside the pore; RBPB's permeability aging is more than 10 times, and the service time is long.
5. The permeable brick made of desert sand and epoxy resin has a permeability coefficient of 3.25×10^{-2} cm/s, a compressive strength of 36.19 MPa and a porosity of 30.39%, and has been produced and applied.

Funding Statement: This work was supported by National Key R & D Program of China (Grant No. 2016YFC0700800).

Conflicts of Interest: The authors declare that they have no conflicts of interest to report regarding the present study.

References

1. Yuan, F., Bauer, M. E. (2007). Comparison of impervious surface area and normalized difference vegetation index as indicators of surface urban heat island effects in landsat imagery. *Remote Sensing of Environment, 106(3),* 375–386. DOI 10.1016/j.rse.2006.09.003.
2. Paul, M. J., Meyer, J. L. (2001). Streams in the urban landscape. *Annual Review of Ecology and Systematics, 32(1),* 333–365. DOI 10.1146/annurev.ecolsys.32.081501.114040.
3. Carlson, T. N., Traci Arthur, S. (2000). The impact of land use—land cover changes due to urbanization on surface microclimate and hydrology: a satellite perspective. *Global and Planetary Change, 25(1),* 49–65. DOI 10.1016/S0921-8181(00)00021-7.
4. Göbel, P., Dierkes, C., Coldewey, W. G. (2007). Storm water runoff concentration matrix for urban areas. *Journal of Contaminant Hydrology, 91(1–2),* 26–42. DOI 10.1016/j.jconhyd.2006.08.008.
5. Miller, J. D., Kim, H., Kjeldsen, T. R., Packman, J., Grebby, S. et al. (2014). Assessing the impact of urbanization on storm runoff in a peri-urban catchment using historical change in impervious cover. *Journal of Hydrology, 515,* 59–70. DOI 10.1016/j.jhydrol.2014.04.011.
6. Connors, J. P., Galletti, C. S., Chow, W. T. L. (2013). Landscape configuration and urban heat island effects: assessing the relationship between landscape characteristics and land surface temperature in Phoenix. *Arizona Landscape Ecology, 28(2),* 271–283. DOI 10.1007/s10980-012-9833-1.
7. Sen, S., Roesler, J. (2019). Thermal and optical characterization of asphalt field cores for microscale urban heat island analysis. *Construction and Building Materials, 217,* 600–611. DOI 10.1016/j.conbuildmat.2019.05.091.
8. Li, H., Harvey, J., Ge, Z. (2014). Experimental investigation on evaporation rate for enhancing evaporative cooling effect of permeable pavement materials. *Construction and Building Materials, 65,* 367–375. DOI 10.1016/j.conbuildmat.2014.05.004.
9. Yuan, X., Tang, Y., Li, Y., Wang, Q., Zuo, J. et al. (2018). Environmental and economic impacts assessment of concrete pavement brick and permeable brick production process—a case study in China. *Journal of Cleaner Production, 171,* 198–208. DOI 10.1016/j.jclepro.2017.10.037.
10. Zhou, C. (2018). Production of eco-friendly permeable brick from debris. *Construction and Building Materials, 188,* 850–859. DOI 10.1016/j.conbuildmat.2018.08.049.
11. Cai, R., Mandula, C. J. (2018). Research on the performance of sand-based environmental-friendly water permeable bricks. *IOP Conference Series: Earth and Environmental Science, 113,* 12136. DOI 10.1088/1755-1315/113/1/012136.

12. Wang, Y., Gao, S., Liu, X., Tang, B., Mukiza, E. et al. (2019). Preparation of non-sintered permeable bricks using electrolytic manganese residue: environmental and NH_3-N recovery benefits. *Journal of Hazardous Materials, 378,* 120768. DOI 10.1016/j.jhazmat.2019.120768.
13. He, T. S., Zhao, X. G., Zhao, S. Y., Li, Z. B., Liu, H. N. (2014). Grey correlation analysis between influence factors and performances of permeable brick. *Bulletin of the Chinese Ceramic Society, 33(8),* 1935–1939 (in Chinese).
14. Trabelsi, A., Slimani, Z., Younsi, A., Virgone, J., Belarbi, R. (2019). Modeling water adsorption and retention of building materials from pore size distribution. *Journal of Renewable Materials, 7(6),* 547–556. DOI 10.32604/jrm.2019.04426.
15. Zhu, M., Wang, H., Liu, L., Ji, R., Wang, X. (2017). Preparation and characterization of permeable bricks from gangue and tailings. *Construction and Building Materials, 148,* 484–491. DOI 10.1016/j.conbuildmat.2017.05.096.
16. Xie, M., Gao, D., Liu, X. B., Li, F., Huang, C. (2012). Utilization of waterworks sludge in the production of fired/unfired water permeable bricks. *Advanced Materials Research, 531,* 316–319. DOI 10.4028/www.scientific.net/AMR.531.316.
17. Shi, H., Ma, H. W., Tian, L. N., Zhang, S. G. (2018). Preparation of permeable paving bricks via geopolymeric method. *Bulletin of the Chinese Ceramic Society, 37(03),* 967–973.
18. He, T. S., Zhao, X. G., Zhao, S. Y., Li, Z. B., Fang, K. N. (2015). Mix proportion design method of permeable brick based on cement paste thickness on coated aggregates. *Journal of Building Materials, 18(2),* 287–290. DOI 10.3969/j.issn.1007-9629.2015.02.017.
19. Haecker, C. J., Garboczi, E. J., Bullard, J. W., Bohn, R. B., Sun, Z. et al. (2005). Modeling the linear elastic properties of Portland cement paste. *Cement and Concrete Research, 35(10),* 1948–1960. DOI 10.1016/j.cemconres.2005.05.001.
20. Dalton, J. L., Gardner, K. H., Seager, T. P., Weimer, M. L., Spear, J. C. M. et al. (2004). Properties of Portland cement made from contaminated sediments. *Resources, Conservation and Recycling, 41(3),* 227–241. DOI 10.1016/j.resconrec.2003.10.003.
21. Jo, B. W., Sikandar, M. A., Chakraborty, S., Baloch, Z. (2017). Strength and durability assessment of Portland cement mortars formulated from hydrogen-rich water. *Advances in Materials Science and Engineering, 2017 (6),* 1–10. DOI 10.1155/2017/2526130.
22. Aouad, G., Laboudigue, A., Gineys, N., Abriak, N. E. (2012). Dredged sediments used as novel supply of raw material to produce Portland cement clinker. *Cement and Concrete Composites, 34(6),* 788–793. DOI 10.1016/j.cemconcomp.2012.02.008.
23. Wheat, H. G. (2002). Using polymers to minimize corrosion of steel in concrete. *Cement and Concrete Composites, 24(1),* 119–126. DOI 10.1016/S0958-9465(01)00032-4.
24. Issa, C. A., Debs, P. (2007). Experimental study of epoxy repairing of cracks in concrete. *Construction and Building Materials, 21(1),* 157–163. DOI 10.1016/j.conbuildmat.2005.06.030.
25. Pour-Ali, S., Dehghanian, C., Kosari, A. (2015). Corrosion protection of the reinforcing steels in chloride-laden concrete environment through epoxy/polyaniline—camphorsulfonate nanocomposite coating. *Corrosion Science, 90,* 239–247. DOI 10.1016/j.corsci.2014.10.015.
26. Selvaraj, R., Selvaraj, M., Iyer, S. V. K. (2009). Studies on the evaluation of the performance of organic coatings used for the prevention of corrosion of steel rebars in concrete structures. *Progress in Organic Coatings, 64(4),* 454–459. DOI 10.1016/j.porgcoat.2008.08.005.
27. Prolongo, S. G., Del Rosario, G., Ureña, A. (2006). Comparative study on the adhesive properties of different epoxy resins. *International Journal of Adhesion and Adhesives, 26(3),* 125–132. DOI 10.1016/j.ijadhadh.2005.02.004.
28. Young, R. J., Beaumont, P. W. R. (1977). Failure of brittle polymers by slow crack growth: part 3 effect of composition upon the fracture of silica particle-filled epoxy resin composites. *Journal of Materials Science, 12 (4),* 684–692. DOI 10.1007/BF00548158.
29. Rao, W., Xu, H., Xu, Y., Qi, M., Liao, W. et al. (2018). Persistently flame-retardant flexible polyurethane foams by a novel phosphorus-containing polyol. *Chemical Engineering Journal, 343,* 198–206. DOI 10.1016/j.cej.2018.03.013.

30. Trovati, G., Sanches, E. A., Neto, S. C., Mascarenhas, Y. P., Chierice, G. O. (2010). Characterization of polyurethane resins by FTIR, TGA, and XRD. *Journal of Applied Polymer Science, 115(1),* 263–268. DOI 10.1002/app.31096.
31. Kostrzewa, M., Hausnerova, B., Bakar, M., Dalka, M. (2011). Property evaluation and structure analysis of polyurethane/epoxy graft interpenetrating polymer networks. *Journal of Applied Polymer Science, 122(3),* 1722–1730. DOI 10.1002/app.34070.
32. Araújo, M. D. V., Pereira, A. S., Oliveira, J. L. D., Brandão, V. A. A., Brasileiro Filho, F. D. A. et al. (2019). Industrial ceramic brick drying in oven by CFD. *Materials, 12(10),* 1612. DOI 10.3390/ma12101612.
33. Dabat, T., Mazurier, A., Hubert, F., Tertre, E., Grégoire, B. et al. (2018). Mesoscale anisotropy in porous media made of clay minerals: a numerical study constrained by experimental data. *Materials, 11(10),* 1972. DOI 10.3390/ma11101972.
34. Kladias, N., Prasad, V. (1991). Experimental verification of Darcy-Brinkman-Forchheimer flow model for natural convection in porous media. *Journal of Thermophysics and Heat Transfer, 5(4),* 560–576. DOI 10.2514/3.301.
35. Markowich, P. A., Titi, E. S., Trabelsi, S. (2016). Continuous data assimilation for the three-dimensional Brinkman-Forchheimer-extended Darcy model. *Nonlinearity, 29(4),* 1292–1328. DOI 10.1088/0951-7715/29/4/1292.
36. Bhatti, M. M., Zeeshan, A., Ellahi, R., Shit, G. C. (2018). Mathematical modeling of heat and mass transfer effects on MHD peristaltic propulsion of two-phase flow through a Darcy-Brinkman-Forchheimer porous medium. *Advanced Powder Technology, 29(5),* 1189–1197. DOI 10.1016/j.apt.2018.02.010.
37. Umavathi, J. C., Ojjela, O., Vajravelu, K. (2017). Numerical analysis of natural convective flow and heat transfer of nanofluids in a vertical rectangular duct using Darcy-Forchheimer-Brinkman model. *International Journal of Thermal Sciences, 111,* 511–524. DOI 10.1016/j.ijthermalsci.2016.10.002.
38. Bouabda, R., Bouabid, M., Ben Brahim, A., Magherbi, M. (2016). Numerical study of entropy generation in mixed MHD convection in a square lid-driven cavity filled with Darcy-Brinkman-Forchheimer porous medium. *Entropy, 18(12),* 436. DOI 10.3390/e18120436.
39. Hdhiri, N., Ben Beya, B. (2018). Numerical study of laminar mixed convection flow in a lid-driven square cavity filled with porous media: Darcy-Brinkman-Forchheimer and Darcy-Brinkman models. *International Journal of Numerical Methods for Heat & Fluid Flow, 28(4),* 857–877. DOI 10.1108/HFF-04-2016-0146.
40. GB/T 2567-2008 (2008). *Test method for properties of resin casting body*. Beijing: Standards Press of China.
41. GB/T 25993-2010 (2010). *Permeable paving bricks & permeable paving flags*. Beijing: Standards Press of China.
42. GB/T 17671-1999 (1999). *Test method for strength of cement mortar*. Beijing: Standards Press of China.
43. GB/T 1040-1992 (1992). Plastics-determination of tensile properties. Beijing: Standards Press of China.
44. Yao, K., Pan, Y., Jia, L., Yi, J. T., Hu, J. et al. (2019). Strength evaluation of marine clay stabilized by cementitious binder. *Marine Georesources & Geotechnology, 1(1),* 1–14. DOI 10.1080/1064119X.2019.1615583.
45. Yao, K., Chen, Q., Xiao, H., Liu, Y., Lee, F. H. (2020). Small-strain shear modulus of cement-treated marine clay. *Journal of Materials in Civil Engineering, 32(6),* 040201146. DOI 10.1061/(ASCE)MT.1943-5533.0003153.
46. Jiang, Z., Sun, Z., Wang, P. (2005). Effects of some factors on properties of porous pervious concrete. *Journal of Building Materials, 8(5),* 513–519 (in Chinese).
47. Kayhanian, M., Anderson, D., Harvey, J. T., Jones, D., Muhunthan, B. (2012). Permeability measurement and scan imaging to assess clogging of pervious concrete pavements in parking lots. *Journal of Environmental Management, 95(1),* 114–123. DOI 10.1016/j.jenvman.2011.09.021.
48. Siriwardene, N., Deletic, A., Fletcher, T. (2007). Clogging of stormwater gravel infiltration systems and filters: insights from a laboratory study. *Water Research, 41(7),* 1433–1440. DOI 10.1016/j.watres.2006.12.040.
49. JG/T 376-2012 (2012). *Sand-based water permeable brick*. Beijing: Standards Press of China.